



Fast Optimization of Arbitrary-shaped Antennas Using a Deep Neural Network Model Trained Once by an Efficient Electromagnetic Field Solver

Downloaded from: <https://research.chalmers.se>, 2026-04-19 06:06 UTC

Citation for the original published paper (version of record):

Maxharraj, F., Maaskant, R., Manholm, L. et al (2025). Fast Optimization of Arbitrary-shaped Antennas Using a Deep Neural Network Model Trained Once by an Efficient Electromagnetic Field Solver. *IEEE Antennas and Wireless Propagation Letters*, 24(12): 4525-4529. <http://dx.doi.org/10.1109/LAWP.2025.3593998>

N.B. When citing this work, cite the original published paper.

© 2025 IEEE. Personal use of this material is permitted. Permission from IEEE must be obtained for all other uses, in any current or future media, including reprinting/republishing this material for advertising or promotional purposes, or reuse of any copyrighted component of this work in other works.

Fast Optimization of Arbitrary-Shaped Antennas Using a Deep Neural Network Model Trained Once by an Efficient Electromagnetic Field Solver

Fitim Maxharraj ¹, Graduate Student Member, IEEE, Rob Maaskant ², Senior Member, IEEE, Lars Manholm ³, Parisa Aghdam ⁴, and Marianna Ivashina ⁵, Senior Member, IEEE

Abstract—Fast optimization of arbitrary-shaped antennas is enabled by a neural network model, trained by a method of moments (MoM) framework capable of evaluating large sets of pixel-based antenna metal layouts. The MoM matrix equation is constructed once for a fully metalized pattern. Matrix rows and columns are selectively removed to reflect the absence of metal pixels. Fixed regions, such as the ground plane, dielectric, and meshed port, are accounted for the Schur complement. Using this framework, a dataset of 2 000 000 antenna configurations is generated in 19 h—a speedup of 13.5 times compared to a plain MoM approach. Meshing is done only once, as opposed to commercial solvers, including meshing the speed advantage is 270 times. A convolutional neural network is trained on this dataset and combined with a genetic algorithm to synthesize various triple-band Wi-Fi 7 antennas, which are experimentally validated. These results demonstrate the real-world applicability of the proposed MoM framework for machine learning-based optimization of arbitrary-shaped antennas.

Index Terms—Antenna synthesis, machine learning (ML), method of moments (MoM), Wi-Fi 7.

I. INTRODUCTION

DESIGNING and optimizing antennas typically rely on computationally intensive full-wave electromagnetic (EM) simulations using commercial solvers, such as Computer Simulation Technology (CST) or High-Frequency Structure Simulator (HFSS), in conjunction with suitable optimization algorithms. Traditionally, the antenna geometry is parameterized, resulting in a tractable low-dimensional optimization problem. To handle more generic, arbitrarily-shaped geometries, pixel-based antenna metal layouts are often optimized using evolutionary algorithms (EAs) [1], [2], [3], [4], [5], [6], [7], [8], [9], [10], [11], [12], [13], [14]. This is computationally expensive: An average simulation time of 1.03 days per design

is reported in [1] and [2] requires 26 h for a single run and 25 h in [14], while custom EM+EA implementations still take 6 h to 20 h per solution [5], [7]. Moreover, eight out of 14 studies do not report convergence times [1], [2], [3], [4], [5], [6], [7], [8], [9], [10], [11], [12], [13], [14].

Machine learning (ML) methods have been explored to reduce the reliance on repeated EM simulations. Neural network models (NNMs) are trained on large datasets of precomputed EM solutions, enabling near-instantaneous prediction of antenna performance and significantly accelerating the optimization process [15], [16], [17]. ML methods have also been integrated with pixel-based synthesis [18], [19], [20], but have only been applied to small datasets, as this becomes the new computational bottleneck. In [18], a dataset of 1940 samples was generated using CST, but only 2–4 pixels were modified, severely restricting the design space. Similarly, Zhang et al. [19] used HFSS to produce 500 samples for a 12×12 grid (solution space: 2^{144}), while Wu et al. [20] proposed an iterative ML-based surrogate model starting from 50 samples. Yet, even in that case, a single optimized design took 26.5 h. Notably, none of these studies validated their models experimentally.

Our group previously introduced a method-of-moments (MoM)-based technique for rapid dataset generation of pixelated antennas [21], which is extended in this letter by the Schur complement enabling the optimization of more complex antenna elements. Large static components of the MoM matrix are pre-computed, such as the ground plane and dielectric layers, and are reused across all simulations, eliminating the need for full matrix reassembly and inversion for each geometry. Antenna-specific variations are handled via fast matrix reductions. The key novel contributions include: 1) a scalable, Schur complement-based MoM method that enables fast EM modeling of complex antennas employing large static regions; 2) efficient generation of large datasets suitable for ML training through fast matrix reduction techniques for pixel-based antenna metals; and 3) demonstration of EM-modeling-free antenna optimization via convolutional neural network (CNN) + genetic algorithm (GA) synthesis and experimental validation of multiband Wi-Fi 7 antennas.

The rest of this letter is organized as follows. Section II presents the methodology, including the MoM framework, data generation, and ML model. Section III presents numerical results comparing a direct MoM approach with our enhanced MoM

Received 9 July 2025; accepted 24 July 2025. Date of publication 30 July 2025; date of current version 18 December 2025. This work was supported by the National Growth Fund through the Dutch 6G flagship project “Future Network Services.” (Corresponding author: Fitim Maxharraj.)

Fitim Maxharraj, Rob Maaskant, and Marianna Ivashina are with the Antenna Group, Department of Electrical Engineering, Chalmers University of Technology, Gothenburg, Sweden (e-mail: fitim@chalmers.se; rob.maaskant@chalmers.se; marianna.ivashina@chalmers.se).

Lars Manholm and Parisa Aghdam are with Ericsson Research, Gothenburg, Sweden (e-mail: lars.manholm@ericsson.com; parisa.aghdam@ericsson.com).

Digital Object Identifier 10.1109/LAWP.2025.3593998

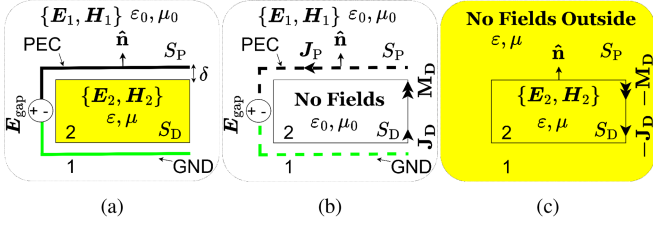


Fig. 1. (a) Original problem where (a) = (b) + (c) and \mathbf{E}_{gap} is a voltage gap source [23]. (b) External equivalent. (c) Internal equivalent.

approach. Section IV discusses experimental validation using water-cut Wi-Fi 7 antennas. Finally, Section V concludes this letter.

II. METHODOLOGY

A. MoM Implementation

Fig. 1(a) shows the original problem with region 1 as $\{\mu_0, \epsilon_0\}$ (vacuum) and region 2 as $\{\mu, \epsilon\}$. Using equivalence principles [22], the original problem is divided into external and internal equivalents shown in Fig. 1(b) and (c). The Poggio–Miller–Chang–Harrington–Wu–Tsai formulation [24] is used, treating the conductor and dielectric as separate regions, with a gap-distance δ [cf., Fig. 1(a)]. Applying boundary conditions lead to integral equations for the unknown currents \mathbf{J}_P , \mathbf{J}_D , and \mathbf{M}_D using the field operators $\{\mathcal{E}_{1,2}, \mathcal{H}_{1,2}\}$ in the respective media, i.e.,

$$\mathcal{E}_1(\mathbf{J}_P) + \mathcal{E}_1(\mathbf{J}_D, \mathbf{M}_D)|_{\text{tan}} = -\mathbf{E}_{\text{gap}}|_{\text{tan}} \quad (1a)$$

$$\mathcal{E}_1(\mathbf{J}_P) + \mathcal{E}_1(\mathbf{J}_D, \mathbf{M}_D) + \mathcal{E}_2(\mathbf{J}_D, \mathbf{M}_D)|_{\text{tan}} = 0 \quad (1b)$$

$$\mathcal{H}_1(\mathbf{J}_P) + \mathcal{H}_1(\mathbf{J}_D, \mathbf{M}_D) + \mathcal{H}_2(\mathbf{J}_D, \mathbf{M}_D)|_{\text{tan}} = 0 \quad (1c)$$

for $\mathbf{r} \in \{S_P, S_D\}$, and where “tan” denotes the tangential component. The local E-field in the voltage-gap port is denoted by \mathbf{E}_{gap} . The left-hand side represents scattered fields and the right-hand side the excitation vector. The perfect electric conductor (PEC) current \mathbf{J}_P , and the dielectric currents $\{\mathbf{J}_D, \mathbf{M}_D\}$ are expanded using N_P and N_D Rao–Wilton–Glisson (RWG) basis functions [25], i.e.,

$$\mathbf{J}_P = \sum_{n=1}^{N_P} I_n^P \mathbf{f}_n^P, \quad \mathbf{J}_D = \sum_{n=1}^{N_D} I_n^{D_j} \mathbf{f}_n^{D_j}, \quad \mathbf{M}_D = \sum_{n=1}^{N_D} I_n^{D_M} \mathbf{f}_n^{D_M} \quad (2)$$

where \mathbf{f}_n^P and $\mathbf{f}_n^{D_j}$ are the n th RWG basis function for \mathbf{J}_P and $\{\mathbf{J}_D, \mathbf{M}_D\}$, respectively, with corresponding expansion coefficient I_n^P , and $\{I_n^{D_j}, I_n^{D_M}\}$. Substituting these expansions into (1) and using Galerkin’s testing method [26] (equal test and basis functions) yield the MoM matrix equation

$$\begin{bmatrix} \mathbf{Z}_{P,P} & \mathbf{Z}_{P,D_j} & \mathbf{Z}_{P,D_M} \\ \mathbf{Z}_{D_j,P} & \mathbf{Z}_{D_j,D_j} & \mathbf{Z}_{D_j,D_M} \\ \mathbf{Z}_{D_M,P} & \mathbf{Z}_{D_M,D_j} & \mathbf{Z}_{D_M,D_M} \end{bmatrix} \begin{bmatrix} \mathbf{I}^P \\ \mathbf{I}^{D_j} \\ \mathbf{I}^{D_M} \end{bmatrix} = \begin{bmatrix} \mathbf{V}^P \\ \mathbf{V}^{D_j} \\ \mathbf{V}^{D_M} \end{bmatrix}. \quad (3)$$

The full complex matrix \mathbf{Z} is of size $N \times N$ and $\{\mathbf{I}, \mathbf{V}\}$ are $N \times 1$ complex-valued vectors, where $N = N_P + 2N_D$.

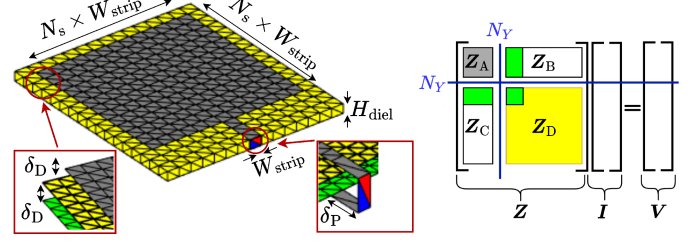


Fig. 2. (Left) Antenna geometry with a delta gap excitation (red/blue), where the gap $\delta_D = 1 \mu\text{m}$ separates the patch/dielectric and ground, port extension $\delta_P = 1 \text{ mm}$, $H_{\text{diel}} = 1.5 \text{ mm}$, $W_{\text{strip}} = 2 \text{ mm}$, and $N_s = 13$, forming a 13×13 patch mesh of size $26 \text{ mm} \times 26 \text{ mm}$. (Right) MoM matrix partitioned at position N_Y ; colors illustrate material regions from (left) (not to scale).

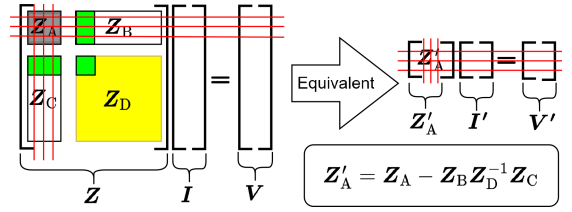


Fig. 3. Original problem where \mathbf{Z} is of size $N \times N$ and the equivalent problem using the Schur complement where \mathbf{Z}'_A is of size $N_Y \times N_Y$.

B. Dielectric Antenna

A patch antenna formed by a 13×13 binary mesh of square elements, each subdivided into two triangles, is placed on a substrate with ground plane as shown in Fig. 2(a). The \mathbf{Z} in Fig. 2(b) is computed once, similar to [21] and [27], furthermore, it is partitioned in the submatrices: \mathbf{Z}_A , which is of size $N_Y \times N_Y$ containing the reaction integrals between the reconfigurable patch, strip, and voltage-gap port RWGs; \mathbf{Z}_D is of size $(N - N_Y) \times (N - N_Y)$ representing the ground-plane and substrate interactions; \mathbf{Z}_B and \mathbf{Z}_C are of size $N_Y \times (N - N_Y)$ and $(N - N_Y) \times N_Y$, respectively, capturing the coupling between \mathbf{Z}_A and \mathbf{Z}_D . In the shown configuration, $N = 6340$ and $N_Y = 516$. The current distribution \mathbf{I}' is of size $N_Y \times 1$, computed using the Schur complement [28]

$$\mathbf{I}' = [\mathbf{Z}_A - \mathbf{Z}_B \mathbf{Z}_D^{-1} \mathbf{Z}_C]^{-1} \mathbf{V}' = [\mathbf{Z}'_A]^{-1} \mathbf{V}' \quad (4)$$

where \mathbf{Z}'_A is only of size $N_Y \times N_Y$ and represents the reconfiguration region while implicitly accounting for the presence of the fixed dielectric and ground plane. Without a fixed region, or including the fixed region in \mathbf{Z}'_A then $\mathbf{Z}'_A = \mathbf{Z}$.

As shown in Fig. 3, the dataset is generated by randomly removing RWGs associated with square elements, as opposed to triangles [21], or zeroing out matrix elements [29]. This is accomplished by eliminating corresponding rows and columns from the original matrix \mathbf{Z}_A (red strikethroughs). The row-column removal process can equivalently be done directly on the original but smaller matrix \mathbf{Z}'_A for a fully metalized pattern. It is computed once and reused across the simulations, reducing computation time while preserving accuracy. Hence, instead of inverting the full 6340×6340 matrix, the reduced system involves inverting matrices up to 516×516 , greatly lowering computational cost. Using a direct lower-upper (LU) decomposition-based solver (Gaussian elimination), the speedup factor scales as $\mathcal{O}((N/N_Y)^3)$.

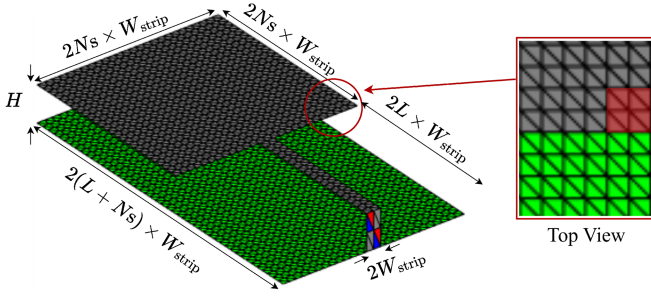


Fig. 4. Geometry of the full metal antenna with height $H = 5$ mm, strip width 2 mm ($W_{\text{strip}} = 1$ mm), and $N_s = 13$, forming a $26 \text{ mm} \times 26 \text{ mm}$ patch. The red box on the right highlights a $2 \text{ mm} \times 2 \text{ mm}$, corresponding to one cell in the 13×13 grid representation of the patch.

Since the gap values $\{\delta_D, \delta_P\}$ are case-dependent, inappropriate choices leads to inaccuracies [30].

C. Metal-Only Antenna

Although numerical validation will be done for a mixed dielectric-metal structure, the Wi-Fi 7 antenna design is a metal-only antenna in air dielectrics for high-radiation efficiency. This also simplifies the formulation to the well-known electric field integral equation in (1a), thus removing dielectric currents and reducing the problem size from N to N_P unknowns.

Removing squares introduces sharp corners requiring finer local meshing for accurate current modeling. Hence, a 26×26 patch grid is used to capture the current, as shown in Fig. 4(left), corresponding to an RWG length of approx. $\lambda/42$ along the shortest edge and $\lambda/30$ along the diagonal. This is a form of submeshing, since the 2×2 highlighted red block in Fig. 4(right) is mapped as PEC or vacuum in a coarser 13×13 mesh for NNM training. The full MoM matrix, of size $(\mathbf{Z}) = 5604 \times 5604$, is computed once and block-partitioned such that $\text{size}(\mathbf{Z}'_A) = 2089 \times 2089$.

D. Data Generation and ML Model

A dataset of 2000000 randomly generated antennas was simulated in 19 h on three nodes at the Chalmers cluster Vera, from 1 GHz to 7 GHz in 100 MHz steps, totaling 61 freq. points. Each antenna has 20%–80% random metal coverage. Furthermore, the dataset contains only antenna configurations in which all pixels are edge-connected (i.e., no point-connected or isolated pixel antennas are included). The dataset was partitioned into 70% for training, 15% for validation, and 15% for testing. The test set is used for evaluating the model's accuracy. This partitioning is common for large datasets, and ensures a balance between effective model training and reliable performance assessment [15], [18], [20], [21]. In contrast, small datasets often omit a validation or test set entirely [31].

The CNN architecture (see Fig. 5) uses 128 filters to capture higher order patterns and a GA is employed for binary optimization. GAs are well-suited for discrete, nondifferentiable design spaces, making them more effective than methods, such as particle swarm optimization or gradient-based approaches [32]. A detailed description of each hyperparameter can be found in [21]. The current model is tailored to the 13×13 configurations with $|S_{11}|$ as output. The model can incorporate additional input parameters (e.g., substrate height, ϵ_r , and mesh variations)

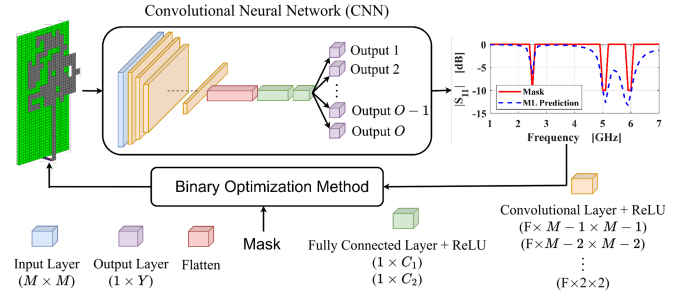


Fig. 5. Generalized CNN model: Input mesh features ($M = 13$), single-output layer ($O = 1$) with $Y = 61$ frequency points. $M - 2$ convolutional layers with $F = 128$ filters and rectified linear unit activation function. Two dense layers ($C_1 = 512$, $C_2 = 256$), Adam optimizer [33], batch size = 1024, and dropout = 0.25, trained for 136 epochs with early stopping.

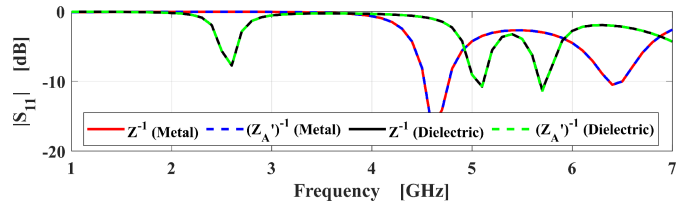


Fig. 6. $|S_{11}|$ for full patched dielectric and metal antenna; \mathbf{Z}^{-1} versus $(\mathbf{Z}'_A)^{-1}$.

and/or outputs (e.g., radiation pattern and efficiency), as shown in [21].

III. NUMERICAL RESULTS

The relative Frobenius norm is used to assess accuracy; for two matrices, \mathbf{A} and \mathbf{B} , it is defined as

$$\epsilon = \frac{\|\mathbf{A} - \mathbf{B}\|_F}{\|\mathbf{B}\|_F} = \frac{\sqrt{\sum_{i=1}^m \sum_{j=1}^n |A_{ij} - B_{ij}|^2}}{\sqrt{\sum_{i=1}^m \sum_{j=1}^n |B_{ij}|^2}} \times 100\%. \quad (5)$$

Fig. 6 shows no visual deviation of the $|S_{11}|$ when results are obtained through the full matrix \mathbf{Z} or the Schur-complement-reduced matrix \mathbf{Z}'_A . This is valid for both the mixed metal-dielectric and metal-only antenna cases, for which $\epsilon = 0.00577\%/1.043 \times 10^{-11}\%$ (single/double precision) and $\epsilon = 0.00316\%/3.784 \times 10^{-10}\%$, respectively. Single precision is used to reduce memory usage and improve the computational efficiency of matrix inversion.

Fig. 7 compares the in-house MoM to the CST-computed $|S_{11}|$ —time domain (TD), frequency domain (FD), and MoM solvers—of the dielectric patch antenna. Differences between the top and bottom figures are primarily due to differences by the solvers in handling the singularities at the sharp corners.

Matrix inversion was performed and timed using a single core of an Intel I9-14900 K processor for the full metal-covered antenna [i.e., Fig. 7 (top)] at 1 GHz and across the 1 GHz–7 GHz range, for both \mathbf{Z} and \mathbf{Z}'_A . In the dielectric case, $\text{size}(\mathbf{Z}) = 6340 \times 6340$ and $\text{size}(\mathbf{Z}'_A) = 516 \times 516$, while for the metal-only case $\text{size}(\mathbf{Z}) = 5604 \times 5604$ and $\text{size}(\mathbf{Z}'_A) = 2089 \times 2089$. The metal-only antenna is meshed twice denser than the dielectric antenna, so \mathbf{Z}'_A for the pixelated metal region ends up larger. Also, the size reduction is different because the fixed region for the dielectric case is relatively large compared

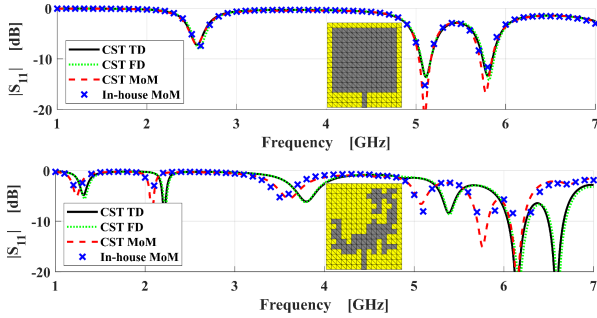


Fig. 7. Comparison between in-house MoM and CST (TD, FD, MoM): (top) full patch, (bottom) random. CST settings, TD: Adaptive mesh with 110 k/256 k cells (top/bottom); FD: 219 k/341 k tetrahedra; MoM: 1300 triangles.

TABLE I
COMPARISON OF MATRIX INVERSION TIMES FOR \mathbf{Z} AND REDUCED SYSTEM \mathbf{Z}'_A FOR FULL METAL-COVERED ANTENNA CONFIGURATIONS

| Antenna | Freq. | \mathbf{Z}^{-1} | $(\mathbf{Z}'_A)^{-1}$ | Speed-up |
|------------|---------|-------------------|------------------------|----------------|
| Dielectric | 1 GHz | 0.5097 s | 0.0042 s | 121.1x (1857x) |
| | 1–7 GHz | 30.839 s | 0.2419 s | 127.5x (1857x) |
| Metal-Only | 1 GHz | 0.8216 s | 0.0746 s | 10.96x (19.3x) |
| | 1–7 GHz | 51.021 s | 3.7682 s | 13.54x (19.3x) |

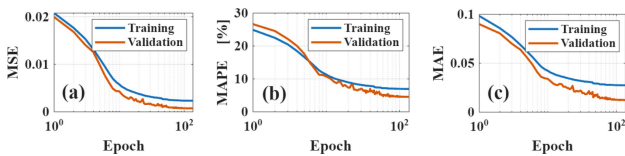


Fig. 8. CNN Training and validation loss: (a) MSE, (b) MAPE, and (c) MAE.

to that of the metal-only antenna. Table I summarizes the results and shows that, in the dielectric case, computational overhead significantly limits the theoretical speedup $\mathcal{O}((N/N_Y)^3)$. The computation of \mathbf{Z}'_A , which includes the inversion of \mathbf{Z}_D , took 50.7 s for the dielectric case and 56.9 s for the metal-only case. Performed only once, this step has negligible impact on total simulation time. It amounts to a $13.5\times$ speedup for the inversion, $20\times$ for the matrix assembly (our previous work [21]), and totaling $270\times$ compared to a plain MoM approach. The ML model was trained on an RTX 4080S GPU (136 epochs, ~ 5.3 min/epoch, ~ 12 h total) until the mean squared error (mse) convergence stalled for 20 epochs. Fig. 8 shows the training and validation loss versus epoch. The model's losses on unseen data are: mse: 7.74×10^{-4} , mean absolute percentage error (MAPE): 4.51%, and mean absolute error (MAE): 0.013. Using the CNN in Fig. 5, which is capable of analyzing thousands of antennas per second, three Wi-Fi 7 antennas were synthesized. Fig. 9 shows a computer-aided design (CAD) model example, radiation pattern, directivity, and efficiency.

IV. EXPERIMENTAL RESULTS

The MoM-CNN-GA framework was used to predict the performance of three metal-only Wi-Fi 7 antennas, each of which was waterjet-cut three times from a 0.4 mm thick brass plate. Each of the nine prototype antennas was soldered to a SubMiniature version A (SMA) connector mounted on the ground plane, the $|S_{11}|$ was measured using Agilent Technologies' VNA model ES071C and electronic calibration module N4431-60006.

Fig. 10 shows good agreement between the ML-predicted, MoM-simulated, and measured $|S_{11}|$, with prototypes operating

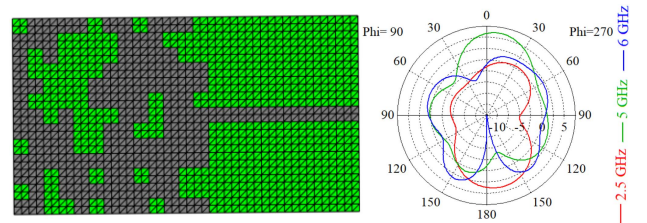


Fig. 9. CAD layout and far-field polar plot ($\phi = 90^\circ$) theta/degrees versus dB (Dir.) of an ML-generated Wi-Fi 7 antenna with $|S_{11}| \leq -10$ dB at 2.5 GHz, 5.0 GHz, and 6.0 GHz, directivities of 4.09 dBi, 6.11 dBi, and 3.67 dBi, respectively, and a simulated radiation efficiency of 99% (-0.03 dB) over the bands.

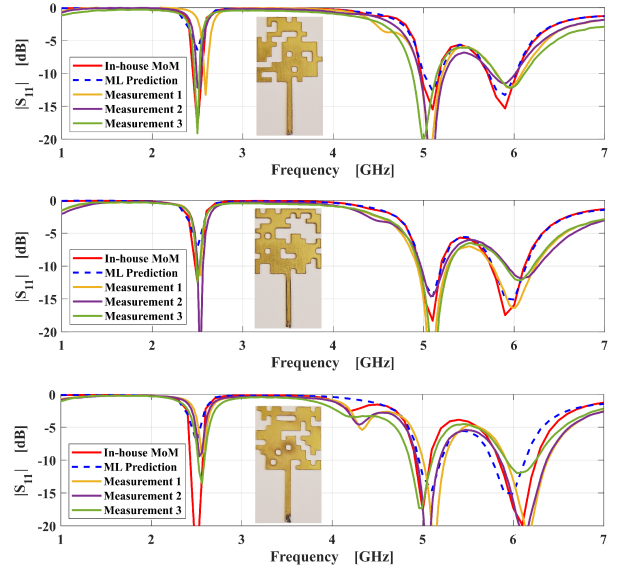


Fig. 10. Measurements of three Wi-Fi 7 antennas, Full-wave simulations, and ML predictions, with a photograph of the brass watercut prototypes in the center.

near the target bands—2.5 GHz (20 MHz/40 MHz bandwidth), 5.0 GHz (80 MHz/160 MHz) and 6.0 GHz (160 MHz/320 MHz). Minor deviations from the $|S_{11}| < -10$ dB threshold are attributed to a 0.5 mm corner-cutting error in fabrication and challenges in manual soldering of metal parts suspended in air, which could be mitigated by printed circuit board (PCB)-based dielectric designs.

V. CONCLUSION

A fast matrix construction and inversion method was presented for the MoM to accelerate dataset generation for ML-based antenna synthesis. A $270\times$ speed-up factor was achieved compared to a plain MoM approach without noticeable accuracy loss.

The ML model achieved an mse of 7.7430×10^{-4} and was used to synthesize three metal-only Wi-Fi 7 antennas with $|S_{11}|$ resonances at 2.5 GHz, 5.0 GHz, and 6.0 GHz. The manufactured prototypes matched the simulation results with minor deviations, demonstrating the practicality of ML-driven antenna design without full-wave solvers during the synthesis.

Future work will explore the use of more efficient NNMs to predict S -parameters and radiation pattern with the help of reduced-order modeling techniques. Additional goals include macrodomain basis function modeling of surface currents and synthesis of large antenna arrays.

REFERENCES

- [1] X. Jia and G. Lu, "A hybrid Taguchi binary particle swarm optimization for antenna designs," *IEEE Antennas Wireless Propag. Lett.*, vol. 18, no. 8, pp. 1581–1585, Aug. 2019.
- [2] A. Ghadimi, V. Nayyeri, M. Khanjarian, M. Soleimani, and O. M. Ramahi, "A systematic approach for mutual coupling reduction between microstrip antennas using pixelization and binary optimization," *IEEE Antennas Wireless Propag. Lett.*, vol. 19, no. 12, pp. 2048–2052, Dec. 2020.
- [3] S. Goudos, "Antenna design using binary differential evolution: Application to discrete-valued design problems," *IEEE Antennas Propag. Mag.*, vol. 59, no. 1, pp. 74–93, Jan. 2017.
- [4] Y.-S. Chen and Y.-H. Chiu, "Application of multiobjective topology optimization to miniature ultrawideband antennas with enhanced pulse preservation," *IEEE Antennas Wireless Propag. Lett.*, vol. 15, pp. 842–845, 2016.
- [5] N. Jin and Y. Rahmat-Samii, "Hybrid real-binary particle swarm optimization (HPSO) in engineering electromagnetics," *IEEE Trans. Antennas Propag.*, vol. 58, no. 12, pp. 3786–3794, Dec. 2010.
- [6] H. Choo and H. Ling, "Design of multiband microstrip antennas using a genetic algorithm," *IEEE Microw. Wireless Compon. Lett.*, vol. 12, no. 9, pp. 345–347, Sep. 2002.
- [7] N. Herscovici, M. Osorio, and C. Peixeiro, "Miniaturization of rectangular microstrip patches using genetic algorithms," *IEEE Antennas Wireless Propag. Lett.*, vol. 1, pp. 94–97, 2002.
- [8] P. Soontornpipit, C. Furse, and Y. C. Chung, "Miniaturized biocompatible microstrip antenna using genetic algorithm," *IEEE Trans. Antennas Propag.*, vol. 53, no. 6, pp. 1939–1945, Jun. 2005.
- [9] R. O. Ouedraogo, E. J. Rothwell, A. Diaz, S.-Y. Chen, A. Temme, and K. Fuchi, "In situ optimization of metamaterial-inspired loop antennas," *IEEE Antennas Wireless Propag. Lett.*, vol. 9, pp. 75–78, 2010.
- [10] A. A. Minasian and T. S. Bird, "Particle swarm optimization of microstrip antennas for wireless communication systems," *IEEE Trans. Antennas Propag.*, vol. 61, no. 12, pp. 6214–6217, Dec. 2013.
- [11] R. Li, D. McNamara, G. Wei, and J. Li, "Increasing radiation efficiency using antenna shape optimization approach," *IEEE Antennas Wireless Propag. Lett.*, vol. 17, no. 3, pp. 393–396, Mar. 2018.
- [12] L. Wang, G. Wang, and J. Sidén, "Design of high-directivity wideband microstrip directional coupler with fragment-type structure," *IEEE Trans. Microw. Theory Techn.*, vol. 63, no. 12, pp. 3962–3970, Dec. 2015.
- [13] J. Dong, Q. Li, and L. Deng, "Design of fragment-type antenna structure using an improved BPSO," *IEEE Trans. Antennas Propag.*, vol. 66, no. 2, pp. 564–571, Feb. 2018.
- [14] B. Thors, H. Steyskal, and H. Holter, "Broad-band fragmented aperture phased array element design using genetic algorithms," *IEEE Trans. Antennas Propag.*, vol. 53, no. 10, pp. 3280–3287, Oct. 2005.
- [15] A. F. Nazmia Kurniawati and S. Alam, "Predicting rectangular patch microstrip antenna dimension using machine learning," *J. Commun.*, vol. 16, no. 9, pp. 394–399, Sep. 2021.
- [16] P. Mukherjee, A. Mukherjee, and K. Chatterjee, "Artificial neural network based dimension prediction of rectangular microstrip antenna," *J. Inst. Engineers (India): Ser. B*, vol. 103, no. 4, pp. 1033–1039, Aug. 2022. [Online]. Available: <https://doi.org/10.1007/s40031-021-00710-6>
- [17] P. Mahouti, "Design optimization of a pattern reconfigurable microstrip antenna using differential evolution and 3D EM simulation-based neural network model," *Int. J. RF Microw. Comput.-Aided Eng.*, vol. 29, no. 8, 2019, Art. no. e21796. [Online]. Available: https://publications.lib.chalmers.se/records/fulltext/166336/local_166336.pdf
- [18] J. P. Jacobs, "Accurate modeling by convolutional neural-network regression of resonant frequencies of dual-band pixelated microstrip antenna," *IEEE Antennas Wireless Propag. Lett.*, vol. 20, no. 12, pp. 2417–2421, Dec. 2021.
- [19] X. Zhang, Y. Tian, and X. Zheng, "Optimal design of fragment-type antenna structure based on PSO-CNN," in *Proc. Int. Appl. Comput. Electromagnetics Soc. Symp. - China (ACES)*, 2019, pp. 1–2.
- [20] Q. Wu, W. Chen, C. Yu, H. Wang, and W. Hong, "Machine-learning-Assisted optimization for antenna geometry design," *IEEE Trans. Antennas Propag.*, vol. 72, no. 3, pp. 2083–2095, Mar. 2024.
- [21] F. Maxharraj, M. Sjödin, R. Maaskant, and M. Ivashina, "Accelerated machine learning antenna synthesis through binary metal-vacuum mesh activation and data reuse in a MoM framework," in *Proc. 19th Eur. Conf. Antennas Propag. (EuCAP)*, 2025, pp. 1–5.
- [22] R. F. Harrington, *Time-Harmonic Electromagnetic Fields*. New York, NY, USA: McGraw-Hill, 1961.
- [23] R. Maaskant, "Analysis of large antenna systems," Ph.D. dissertation, Dept. Elect. Eng., Eindhoven Univ. Technol., Eindhoven, The Netherlands, 2010.
- [24] E. Arvas, A. Rahhal Arabi, A. Sadigh, and S. Rao, "Scattering from multiple conducting and dielectric bodies of arbitrary shape," *IEEE Antennas Propag. Mag.*, vol. 33, no. 2, pp. 29–36, Feb. 1991.
- [25] S. Rao, D. Wilton, and A. Glisson, "Electromagnetic scattering by surfaces of arbitrary shape," *IEEE Trans. Antennas Propag.*, vol. AP-30, no. 3, pp. 409–418, Mar. 1982.
- [26] W. J. Duncan, A. M. A. R. Committee, and G. B. A. R. Committee, Galerkin's Method, Majesty's Stationary Office, London, A.R.C. Tech. Rep. 1798 (3287), 1937.
- [27] S. Bosák, M. Čapek, and J. Matas, "Q-factor evaluation accelerated by a deep neural network," in *Proc. 19th Eur. Conf. Antennas Propag. (EuCAP)*, 2025, pp. 1–5.
- [28] J. Schur, "Über potenzreihen, die im innern des einheitskreises beschränkt sind," *J. für Die Reine Und Angewandte Mathematik*, vol. 1917, no. 147, pp. 205–232, 1917. [Online]. Available: <https://doi.org/10.1515/crll.1917.147.205>
- [29] M. Čapek, L. Jelinek, and M. Gustafsson, "Shape synthesis based on topology sensitivity," *IEEE Trans. Antennas Propag.*, vol. 67, no. 6, pp. 3889–3901, Jun. 2019.
- [30] W.-J. Zhao, L.-W. Li, and K. Xiao, "Analysis of electromagnetic scattering and radiation from finite microstrip structures using an EFIE-PMCHWT formulation," *IEEE Trans. Antennas Propag.*, vol. 58, no. 7, pp. 2468–2473, Jul. 2010.
- [31] Y. Liu and C. D. Sarris, "A convolutional neural network based method for accurate computation of scattered fields from reconfigurable intelligent surfaces," *IEEE Trans. Antennas Propag.*, vol. 73, no. 4, pp. 2615–2627, Apr. 2025.
- [32] J. Robinson and Y. Rahmat-Samii, "Particle swarm optimization in electromagnetics," *IEEE Trans. Antennas Propag.*, vol. 52, no. 2, pp. 397–407, Feb. 2004.
- [33] D. P. Kingma and J. Ba, "Adam: A method for stochastic optimization," 2017. [Online]. Available: <https://arxiv.org/abs/1412.6980>